

# Fitting a Collider in a Quantum Computer: Tackling the Challenges of Quantum Machine Learning for Big Datasets

Miguel Caçador Peixoto<sup>1</sup>, Nuno Filipe Castro<sup>1, 2</sup>, Miguel Crispim Romão<sup>1, 3</sup>,  
Maria Gabriela Jordão Oliveira<sup>1</sup> and Inês Ochoa<sup>4</sup>

<sup>1</sup> LIP – Laboratório de Instrumentação e Física Experimental de Partículas, Escola de Ciências, Campus de Gualtar, Universidade do Minho, 4701-057 Braga, Portugal

<sup>2</sup> Departamento de Física, Escola de Ciências, Campus de Gualtar, Universidade do Minho, 4701-057 Braga, Portugal

<sup>3</sup> Department of Physics and Astronomy, University of Southampton, SO17 1BJ Southampton, United Kingdom

<sup>4</sup> LIP – Laboratório de Instrumentação e Física Experimental de Partículas, Av. Prof. Gama Pinto, 2, 1649-003 Lisboa, Portugal

December 5, 2022

## Abstract

Current quantum systems have significant limitations affecting the processing of large datasets and high dimensionality typical of high energy physics. In this work, feature and data prototype selection techniques were studied to tackle this challenge. A grid search was performed and quantum machine learning models were trained and benchmarked against classical shallow machine learning methods, trained both in the reduced and the complete datasets. The performance of the quantum algorithms was found to be comparable to the classical ones, even when using large datasets.

## 1 Introduction

The Standard Model of Particle Physics (SM) provides a remarkable description of the fundamental constituents of matter and their interactions, being in excellent agreement with the collider data accumulated so far. Nonetheless, there are still important open questions, unaddressed by the SM, such as gravity, dark matter, dark energy, or the matter-antimatter asymmetry in the universe [1], motivating a comprehensive search program for new physics phenomena beyond the SM (BSM) at the Large Hadron Collider (LHC) at CERN.

The search for BSM phenomena at colliders poses specific challenges in data processing and analysis, given the extremely large datasets involved and the low signal to background ratios expected. In this context, the analysis of the collision data obtained by the LHC experiments often relies on machine learning (ML), a field in computer science that can harness large amounts of data to train generalizable algorithms for a variety of applications [2, 3], such as classification tasks. These techniques have shown an outstanding ability to find correlations in high-dimensional parameter spaces to discriminate between potential signal and background processes. They are known to scale with data, and usually rely on a large number of learnable parameters to achieve their remarkable performance.

In order to train these large models, classical<sup>1</sup> machine learning (CML) takes advantage of hardware accelerators, such as graphics processing units (GPUs), for efficient, parallel, and fast matrix multiplications. On the other hand, a new class of hardware is becoming available, with the advent of noisy

---

<sup>1</sup>Classical is used throughout the paper as opposed to *quantum* machine learning.

intermediate-scale quantum (NISQ) computing devices. This accelerated the development of new quantum algorithms targeted at exploiting the capacity and feasibility of this new technology for ML applications.

Quantum machine learning (QML) is an emerging research field aiming to use quantum circuits to tackle ML tasks. One of the motivations for using this new technology in HEP relates to the intrinsic properties of quantum computations, namely representing the data in a Hilbert space where the data can be in a superposition of states or in entangled states, which can allow to explore additional information in data analysis and, eventually, contribute to better classification of HEP events, namely in the context of the search for BSM phenomena. Recently, this new technology has been applied to HEP problems such as event reconstruction [4–10] and classification [11–19].

Despite of the promising potential of quantum computation, the NISQ processors have important limitations, such as the qubit quality, *i.e.* the accuracy with which it is possible to execute quantum gates, the qubit lifetime and the limited depth of quantum circuits, since for large circuits the noise overwhelms the signal [20, 21]. A possible solution to these obstacles is the use reduced data, both in the number of considered features and events to be processed. Since the typical HEP datasets are quite large, these two types of reductions will be explored in this paper, by considering different strategies: ranking of features, data transformations aiming for a richer reduced set of features, use of random samples, and choice of representative data samples. Such studies will be done in a specific HEP context: the search for BSM phenomena in events with multiple leptons and  $b$ -tagged jets, which can be used to achieve a reasonable signal to background ratio. A benchmark BSM signal, leading to the  $Zt$  final state will be considered. The use of QML algorithms in the HEP context was studied, focusing on a binary classification task for the considered BSM signal against SM background. For this purpose, a grid search will be performed on variational quantum classifiers (VQC) by varying adjustable parameters, which can be learned. A classical baseline for comparison was also used. The choice in the current study was to focus on shallow CML methods rather than state-of-the-art architectures based on neural networks (NN). The rationale for this choice is to provide a fair comparison between methodologies, since NN are known to require big data to achieve good performance, in particular if one considers deep NN, which is not feasible given the limitations of the present quantum computers.

## 2 Quantum Machine Learning

QML algorithms are implemented using a quantum circuit, *i.e.* a collection of quantum gates applied to an  $n$ -qubit quantum state, followed by a measurement (or multiple measurements) that represent the output of the circuit. In order to implement a learning algorithm, the quantum circuit can be parameterized with parameters that can be learned by confronting the measurement to a loss function.

QML is effectively an extension of CML techniques to the Hilbert space, where instead of representing data as vectors in a high-dimensional real space, we encode it in state vectors of a Hilbert space. A QML algorithm, such as a quantum neural network, can be implemented using the quantum equivalent of a perceptron, one of the building blocks of CML. A problem arises from the realization that the activation functions used in CML can not be expressed using a linear operation, which is inherently required from the quantum evolution of a state. Ideas have been proposed to imitate an activation function in the quantum space, [22, 23] but, in the current paper, only variational quantum classifiers [24, 25] are used for binary classification.

A VQC is a parameterized quantum circuit, a circuit type containing adjustable gates with tunable parameters. These gates are a universal set of quantum gates and, in the current study, rotation  $[R_X(w), R_Y(w), R_Z(w)]$  and CNOT gates are used<sup>2</sup>.

<sup>2</sup>Even if, in general, the phase shift gate  $P(w)$  should be included, this gate does not change the final outcome (*i.e.* it does not

The considered VQC pipeline used has the following components:

- **Data Embedding:** the numerical vector  $X$  representing the classical information is converted to the quantum space with the preparation of an initial quantum state,  $|\psi_X\rangle$ , which represents a HEP event.
- **Quantum circuit:** a unitary transformation  $U(w)$ , parameterized by a set of free parameters  $w$ , is applied to the initial quantum state  $|\psi_X\rangle$ . This produces the final state  $|\psi'_X\rangle = U(w)|\psi_X\rangle$ .
- **Final prediction:** a measurement of an observable is performed in one of the qubits of the state  $|\psi'_X\rangle$ , which will give the prediction of the model for the task at hand. The training of a VQC aims to find the best set of parameters  $w$  to match the event labels to the prediction.

## 2.1 Data Embedding

Before passing the data through the VQC, the preparation of the initial quantum state  $|\psi_X\rangle$  is required. This is called data embedding, and there are a number of proposals to perform this step [26]. The angle embedding was tested and preliminary results found to lead to a better performance than amplitude embedding, as reported before [17]. This embedding was therefore the choice for the studies reported in this paper.

For an  $N$ -dimensional vector of classical information,  $X = (x_1, x_2, \dots, x_N)$ , the state entering the VQC will be defined via a state preparation circuit applied to the initial ground state  $|0\rangle^{\otimes N}$ . The information contained in  $X$  is embedded as angles: these are the values used in rotation gates applied to each qubit, thus requiring  $N$  qubits for embedding  $N$  features from the original dataset.

In the current study, the embedding is done using rotations around the  $x$ -axis on the Bloch sphere, thus defining the quantum state embedded with the classical information as:

$$|\psi_X\rangle = \bigotimes_{i=1}^N R_X(x_i) = \bigotimes_{i=1}^N \left[ \cos\left(\frac{x_i}{2}\right)|0\rangle - i \sin\left(\frac{x_i}{2}\right)|1\rangle \right], \quad (1)$$

where  $R_X(x) = e^{-ix\hat{\sigma}_x}$  and  $\hat{\sigma}_x$  is a Pauli operator. In this embedding each of the considered features of the original dataset is required to be bound between  $[-\pi, \pi]$ .

## 2.2 Model Circuit

The model circuit is the key component of the VQC and includes the learnable set of parameters. It is defined by a parameterized unitary circuit  $U(w)$ , with  $w$  being the set of tunable parameters, which will evolve a quantum state embedded with classical information  $\psi_X$  into the final state  $\psi'_X$ .

Analogously to the architecture of a classical neural network, the model circuit is formed by layers. Each layer is composed of an assemblage of rotation gates applied to each qubit in the system, followed by a set of CNOT gates.

A rotation gate,  $R$ , is designed to be applied to one single qubit and rotate its state. It is composed by 3 learnable parameters:  $\phi, \theta, \omega$ , which enables the gate to rotate any arbitrary state to any location on the Bloch sphere.

$$R(\phi, \theta, \omega) = RZ(\omega)RY(\theta)RZ(\phi) = \begin{bmatrix} e^{-i(\phi+\omega)/2} \cos(\theta/2) & -e^{i(\phi-\omega)/2} \sin(\theta/2) \\ e^{-i(\phi-\omega)/2} \sin(\theta/2) & e^{i(\phi+\omega)/2} \cos(\theta/2) \end{bmatrix} \quad (2)$$

---

impact probabilities), so it can be discarded.

Since all the learnable parameters of the VQC are contained inside the rotation gates, and each gate has 3 parameters, the shape of the weight vector is  $w \in \mathbb{R}^{n \times l \times 3}$ , where  $n$  is the number of qubits of the current system and  $l$  is the number of layers in the network. As mentioned in the previous section,  $n$  will depend on the number of features in the data and  $l$  is a hyper-parameter (HP) to be tuned.

After rotating the qubits' state, a collection of CNOT gates will be applied to entangle the qubits. The CNOT gate is a 2-qubit gate with no learnable parameters. It will flip the state of the so-called target-qubit, based on the value of the control-qubit, and it is usually represented by having two inputs as such: CNOT(control-qubit, target-qubit). Given the number of qubits, the CNOT arrangement is implemented as detailed in [Algorithm 1](#).

---

**Algorithm 1** CNOT Arrangement

---

**Require:**  $n \geq 2$ ,  $n$  being the number of qubits.

```

if  $n == 2$  then
    CNOT(1,0)
else
    for  $qubit \leftarrow 0$  to  $n-1$  do
        if  $qubit == n-1$  then
            CNOT( $qubit$ ,0)
        else
            CNOT( $qubit$ , $qubit+1$ )
        end if
    end for
end if

```

---

## 2.3 Final prediction

The output of the model is obtained by measuring the expectation value of the Pauli  $\hat{\sigma}_z$  operator in one of the qubits of the final state  $\psi'_X$ . An example of the implementations of a VQC is represented in [Figure 1](#).

## 3 Classical Machine Learning Methods

Shallow CML methods are used to provide a baseline comparison to the QML models. The specific methods chosen for the comparison are Logistic Regression (LR) and Support Vector Machines (SVM), with these algorithms being trained with the same data as the QML algorithms.

All the classical methods were implemented using *scikit-learn* [27] library and, if not specified otherwise, the default parameters were used.

### 3.1 Logistic Regression

Logistic Regression is one of the simplest ML models and can be formulated as one of the basic building blocks of a neural network - a single-layer perceptron. The goal is to find the best set of weights  $w$  that fit the data  $x$ :

$$\hat{y}(w, b, x) = \sigma(w \cdot x + b), \quad (3)$$

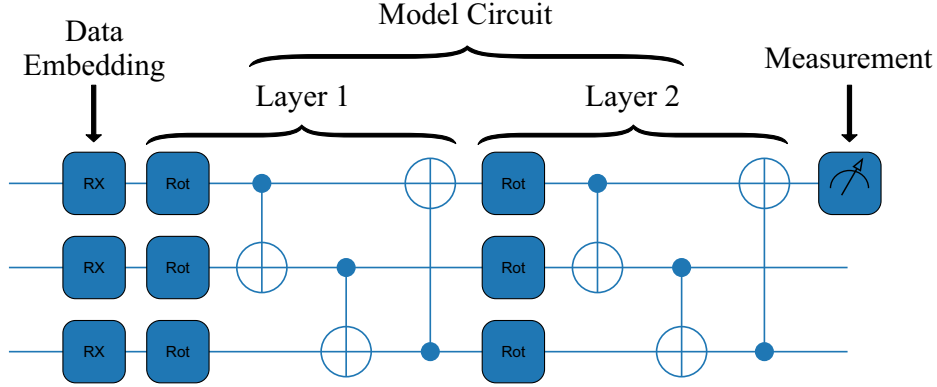


Figure 1: An example circuit for the VQC architecture used. It is comprised of 2 layers and 3 features as input. The three main stages of a QML model can be seen: embedding of the data, passing the data through the model circuit, and the measurement of the outcome.

where  $\hat{y}$  is the probability of an event to belong to class 1,  $w$  and  $b$  are learnable parameters, and  $\sigma$  is the sigmoid function.

The learning process is guided by minimizing the loss function, which in our case is the binary cross-entropy:

$$L = -\mathbb{E}_x[y \log(\hat{y}) + (1 - y) \log(1 - \hat{y})], \quad (4)$$

where  $y$  is the binary label of whether the event is of the class signal or not, and  $\mathbb{E}_x$  is the expectation value over the training data, obtaining using the event weights corresponding to each signal and background process.

### 3.2 Support Vector Machine

An SVM classifier is trained by finding the hyperplane that best separates two classes of data in the hyperspace of features. It does so by using support vectors, which are the data points from the two classes closer to the hyperplane, influencing the position and orientation of the hyperplane.

The loss function of an SVM revolves around the goal of maximizing the margin, *i.e* the distance between the hyperplane and the nearest data point from either class. In other words, the goal is to find the hyperplane with the greatest possible margin between itself and any point within the training set, giving a greater chance of new data being classified correctly.

Just like the Logistic Regression, the base SVM classifier can only learn a linear boundary condition. However, classification problems are rarely simple enough for it to be separable using a hyperplane, thus usually requiring a non-linear separation. SVM can do this by transforming the data using a non-linear function, named kernel, after which it can be split by a hyperplane. For this implementation, the radial-basis function (RBF) was used as kernel. This endows the SVM with a non-linear mapping where it better separates the two classes using a hyperplane.

## 4 Dataset

The dataset used in this work [28] is comprised of simulated events of  $pp$  collisions at 13 TeV, in final states with 2 leptons, at least 1  $b$ -jet, at least 1 large- $R$  jet and large scalar sum of transverse<sup>3</sup> momentum ( $p_T$ ) of all reconstructed particles in the event ( $H_T > 500$  GeV). Such basic selection corresponds to a topology commonly used in different searches for BSM events at the LHC [29]. The dominant SM background for this topology,  $Zb\bar{b}$ , and the BSM signal corresponding to  $t\bar{t}$  production with one of the top-quarks decaying via a flavour changing neutral current decay  $t \rightarrow qZ$  ( $q = c, u$ ) [30], were considered. Such signal was chosen given the kinematic similitude to the background, thus providing a good benchmark for the present study.

Both samples were generated with MADGRAPH5 2.6.5 [31] and PYTHIA 8.2 [32], and the detector was simulated using DELPHES 3 [33] with the default CMS card. Jets were clustered using the anti- $k_t$  algorithm [34] with  $R$ -parameters of 0.5 and 0.8 (the latter for the large- $R$  jets).

The following features were used for training of both the classical and quantum machine learning algorithms:

- $(\eta, \phi, p_T, m, b - tag)$  of the 5 leading jets, ordered by decreasing  $p_T$ , with  $b - tag$  being a Boolean variable indicating if the jet is identified as originating from a  $b$ -quark by the  $b$ -tagging algorithm emulated by DELPHES;
- $(\eta, \phi, p_T, m)$  of the leading large- $R$  jet;
- $N$ -subjettiness of leading large- $R$  jet,  $\tau_n$  with  $n = 1, \dots, 5$  [35].
- $(\eta, \phi, p_T)$  of the 2 leading leptons (electrons or muons);
- transverse momentum ( $\cancel{E}_T$ ) and  $\phi$  of the missing transverse energy;
- multiplicity of jets, large- $R$  jets, electrons and muons;
- $H_T$ .

The proportion of signal and background events was kept the same as the original simulated data during training, being 12.94% and 87.06% respectively. Additionally, the Monte Carlo weights, corresponding to the theoretical prediction for each process at target luminosity of  $150 \text{ fb}^{-1}$ , were taken into account in the evaluation of all the considered metrics and loss functions.

## 5 Feature Selection

As described in the previous section, a total of 47 features are available for training. Considering the type of data embedding chosen, 47 qubits would be needed to train a VQC using all the dataset features. Such number of qubits is impractical given the currently available quantum computers and thus it is not feasible to train a VQC using all the features in our dataset. For the purposes of the current study, quantum computers with only 5 qubits were considered and two methods for feature selection were implemented: principal component analysis (PCA) and sequential feature selection (SFS).

A relative comparison of the best 5 features<sup>4</sup> is shown in Table 1 while the best performance obtained with state-of-the-art CML methods without any features or data points restrictions can be seen in Figure 2.

<sup>3</sup>The transverse plane is defined with respect to the proton colliding beams.

<sup>4</sup>The area under the curve (AUC) of the receiver operating characteristic curve (ROC) is considered as metric for these comparisons.

Feature	AUC
$\cancel{E}_T$	0.817
Lepton <sub>1</sub> $p_T$	0.692
Lepton <sub>2</sub> $p_T$	0.649
large- $R$ jet $m$	0.609
large- $R$ jet $\tau_1$	0.576

Table 1: Top 5 features ranked by their AUC Score on the training dataset.

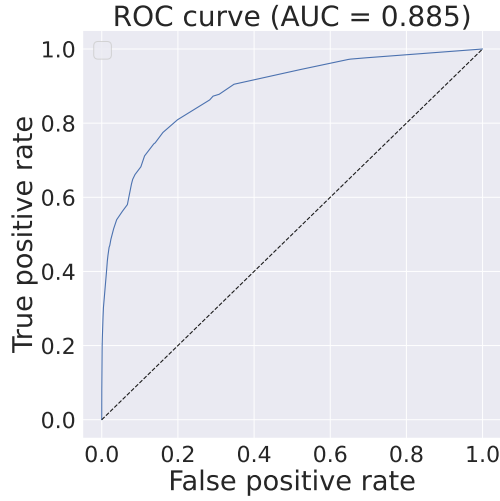


Figure 2: Obtained ROC curve and respective AUC score on the test dataset when training an Boosted Decision Tree, implemented with *xgboost* [36] using the full set of features and data points. The classifier has an identical configuration as the one described in [subsection 5.1](#).

## 5.1 Sequential Feature Selection

SFS algorithms are a widely used family of greedy search algorithms used for automatically selecting a subset of features that is most relevant to the problem. This is achievable by removing or adding one feature at a time based on the classifier performance until a feature subset of the desired size,  $k$ , is reached.

There are different variations of SFS algorithms but for the current paper, the Sequential Backward Selection (SBS) algorithm was chosen. This algorithm starts with the full set of features ( $n = 47$ ) and, at each iteration, it generates all possible feature subsets of size  $n - 1$  and trains a ML model for each one of the subsets. The performance is subsequently evaluated and the feature that is absent from the subset of features with the highest performance metric is removed. This process is iterated until the feature subset contains  $k$  features.

This technique was used to find subsets of 1 to 5 features. The ML model assisting the SBS was a boosted decision tree (BDT) with a maximum number of estimators set at 100 and a learning rate of  $1 \times 10^{-5}$ . The considered loss function was a logistic regression for binary classification and the AUC score was used as evaluation metric. The BDT was implemented using *xgboost* [36] and the SBS algorithm

using *mlxtend* [37]. The selected features for the different values of  $k$  is shown in Table 2 and the AUC scores for each feature in Table 3.

$k$	Selected Features
1	$\cancel{E}_T$
2	$\cancel{E}_T$ , Number of muons
3	$\cancel{E}_T$ , Number of muons, $\text{Jet}_1 \text{ } b\text{-tag}$
4	$\cancel{E}_T$ , Number of muons, $\text{Jet}_1 \text{ } b\text{-tag}$ , $\text{Jet}_2 p_T$
5	$\cancel{E}_T$ , Number of muons, $\text{Jet}_1 \text{ } b\text{-tag}$ , $\text{Jet}_2 p_T$ , large- $R \text{ } \tau_3$

Table 2: List of the features selected by the SBS algorithm for  $k = 1, \dots, 5$ .

Feature	AUC
$\cancel{E}_T$	0.817
Number of muons	0.534
$\text{Jet}_1 \text{ } b\text{-tag}$	0.418
large- $R \text{ jet } \tau_3$	0.316
$\text{Jet}_2 p_T$	0.313

Table 3: Features selected by the SBS Algorithm and their respective AUC Score on the training dataset.

## 5.2 Principal Component Analysis

The PCA transforms a highly correlated, high-dimensional dataset and into a new one with reduced dimensionality and uncorrelated features, by rotating the dataset in the direction of the eigenvectors of the dataset covariance matrix. In the present paper, the PCA was performed only to remove the correlation between the features, maintaining the same dimensionality as the original data. The PCA transformation was learned from the training dataset and then applied to all datasets. When training a VQC for a specific number of features, the PCA components were ranked by AUC score and thus selected from the highest to the lowest. This is done by introducing a priority queue, *i.e.* if training a model using two features is desired, the 2 top-ranked PCA components will be selected. The *scikit-learn* PCA implementation was used and the obtained 5 better components are shown in Table 4.

PCA Component	AUC
Component 3	0.726
Component 14	0.606
Component 5	0.565
Component 41	0.563
Component 43	0.560

Table 4: Top 5 PCA components obtained with the training dataset, ranked by their AUC.

## 6 Dataset Size Reduction

The present paper addresses the use of reduced datasets to overcome the limitation of *NISQ* processors while minimizing the loss of information and thus avoiding a performance loss of the QML algorithms in

the HEP context. The primary method used for this purpose in the current study is *KMeans*, where the  $k^{th}$  most representative points, *i.e.* a set of *centroids*, is obtained from the original dataset. Although these *centroids* are the most representative data points, they are not necessarily contained in the original dataset and, consequently, a resampling process, allowing to choose points of the original dataset (centrus), is required.

A study of the performance of the proposed dataset reduction method will be done by training a logistic regression model with the original dataset and comparing the results with those obtained when *Kmeans* and randomly undersampled datasets are used.

## 6.1 KMeans Algorithm

Considering a clustering algorithm, *Kmeans* iteratively tries to separate data into independent groups [38]. This separation is done using the *Lloyd's algorithm* [39], based on the minimal variability of samples within each cluster. The *KMeans* algorithm requires the specification of the desired number of clusters ( $k$ ) a priori. The following steps were used:

1. **Initialization of the centroids:** using the *scikit-learn* implementation, it is possible to do it in two different ways, *random* and *k-means++* [40]:

- **Random:**  $k$  random samples of the original dataset are chosen.
- **K-means++:**  $k$  samples of the original dataset are chosen based on a probabilistic approach, leading to the centroids being initialized far away from each other.

Assuming there is enough time, the algorithm will always converge, although the convergence to an absolute minimum is not guaranteed. The *K-means++* initialization helps to address this issue. Furthermore, for both initializations, the algorithm, by default, runs several times with different centroid seeds, with the best result being the output.

2. **Assignment:** Each data point  $x_{i:}$  is addressed to a cluster  $c_{k'}$ , in such a way that the *inertia* is minimized:

$$k' = \underset{k}{\operatorname{argmin}} \left\{ \sum_{j=0}^{F-1} (x_{ij} - \mu_{kj})^2 \right\}, \quad (5)$$

where  $F$  is the dimensionality, *i.e.* the number of features,  $\mu_k$  is the centroid of the cluster  $c_k$  and  $j$  stands for the  $(j + 1)^{th}$  feature.

3. **Update of the centroids' position:** The new centroids are just the means positions of each cluster, *i.e.*

$$\mu_{k:} = \frac{\sum_{i=0, x_{i:} \in c_k}^{n_k-1} x_{i:}}{n_k}, \quad (6)$$

with  $n_k$  being the number of samples addressed to  $c_k$ . It should be noted that if  $n_{k'} = 0$  the centroid  $\mu_{k'}$  doesn't change.

4. **Iteration:** Steps 2 and 3 are repeated until the maximum number of iterations is reached or until the result converges, *i.e.* the centroids don't change.

The *KMeans* algorithm was used separately for the signal and background samples, with the corresponding weights being used.

## 6.2 Dataset Resampling

As previously mentioned, although centroids are the most representative points, they are not necessarily contained in the original dataset. Hence, it was chosen to consider 10 neighbors of each centroid to determine each centrus, *i.e.* the 10 nearest points of the original dataset.

The position of each centrus was determined using the weighted mean of the position of the neighbors,

$$W = \frac{\sum_{i=0}^9 x_{i:} \times w_i}{\sum_{i=0}^9 w_i}, \quad (7)$$

where  $W$  is the mean position,  $x_{i:}$  is the  $(i + 1)^{th}$  nearest point and  $w_i$  the weight of the sample.

The sample weight of each centrus was calculated based on the number of samples of the same label (*i.e.* signal or background) on the original dataset:

$$w_i = \frac{1}{n}, \quad (8)$$

with  $w_i$  being the weight of the  $(i + 1)^{th}$  centrus and  $n$  the number of samples in the original dataset with the same label of this centrus.

## 7 Quantum and Classical Machine Learning Training

The training of the QML algorithms used in the current paper requires the use of optimizers. Two different ones were considered: *Adam* [41] and tree-structured Parzen estimator sampler (*TPE*) [42, 43].

The *Adam* optimizer uses an extension of stochastic gradient descent, leveraging techniques such as adaptive moment estimation, being extensively used in optimization problems, namely in the context of machine learning. Nonetheless, since there is no reason to expect, *a priori*, that it will work equally well in the context of QML, where specific challenges are expected, the *TPE* optimizer was also tested.

The *TPE* is a Bayesian optimization algorithm first developed for HP tuning in the context of machine learning. In the current studies, it will be used to optimize VQC weights in a way very similar to what is typically done for HP tuning. *TPE* is implemented using *Optuna* [44], a library focused on HP optimization for machine learning models. *TPE* works by choosing a parameter candidate that maximizes the likelihood ratio between a Gaussian Mixture Model (GMM) fitted to the set of parameters associated with the best objective values, with another GMM being fitted to the remaining parameter values. In the context of HEP, *TPE* has also been used to explore parameter spaces of BSM models [45].

For each optimizer, different machine learning methods were considered, namely a LR, a SVM and a VQC. The corresponding training was done for the set of HP summarized in Table 5, where the considered grid of values used in the optimization is also listed. For each set of HP, 5 models of each class were trained on 5 different subsets of the initial dataset (random sampling).

Variable HP	Possible values
Feature Selection	[PCA, SBS]
Number of Data points	[100, 500, 1k, 5k]
Number of Features	[1, 2, 3, 4, 5]
Number of Layers	[1, 2, 3, 4, 5]
Fixed HP	Fixed values
Max Epochs	500
Batch Size	Size of the dataset
Learning Rate (LR)	0.03

Table 5: List of scanned hyperparameters. The LR parameter is used only for the VQC optimized by Adam while the number of layers is only used by the VQCs.

For both optimizers, the considered cost function used is the squared error, with the individual Monte Carlo samples being properly weighted. During the training of VQCs, the inference was done on the validation dataset at 5 epoch intervals, the AUC computed and only the best-performing model, according to the previously mentioned metric, was considered.

## 7.1 Adam Implementation Details

The training starts with the initialization of the weight vector. This is done randomly with an order of magnitude of  $10^{-2}$ , which is followed by training iterations until a maximum number of epochs is reached. At each iteration, the model is inferred with the training dataset, the cost function calculated and the model parameters updated via the *Adam* optimizer. A summary of *Adam*-optimized VQC training is shown in [Algorithm 2](#).

---

### Algorithm 2 Adam Training

---

```

params ← params_initialization()
for epoch ← 1 to max_epochs do
    loss ← cost(params)
    params ← optimizer.step()
    if epoch_number%5 == 0 or epoch_number == max_epochs then
        validation_step()
    end if
end for

```

---

## 7.2 TPE Implementation Details

We use the *Optuna* implementation of the *TPE* sampler. Being a Bayesian optimization algorithm, *TPE* works very differently to *Adam*, which is a gradient descent algorithm. In *TPE*, for every training iteration, each parameter is replaced by a new value acquired sampling from a Gaussian Mixture Model of good points, which is then used to compute the loss function. At each epoch, the algorithm computes new values for the model parameters. With the value of the loss function of the suggested parameters, *TPE* will update its internal Gaussian Mixture Models of good and bad points, which will allow it to learn what are good suggestions as more parameter values are sampled. Since *TPE* is a Bayesian algorithm, it

does not need to compute derivatives of the loss function, as *Adam* does, which might allow for a light workload when running trainings on quantum computers.

### 7.3 Simulation Environment

Throughout this work, the *PennyLane* package [46] was used for hybrid quantum-classical machine learning applications. *PennyLane*'s `default.qubit` quantum simulator – a simple simulator for quantum circuits – was used to train and evaluate the performance of the different QML algorithms. Later, the performance of the trained algorithms will be measured on IBM's quantum computers using *PennyLane* integration with IBM quantum computing framework, *Qiskit* [47].

## 8 Simulation Results

### 8.1 Feature Selection

It was observed that the circuits trained with SBS data are more unstable and show overall worse performance when compared to PCA (except when using only 1 feature), as shown in Figure 3. Furthermore, it was also observed that a small numerical error, even at the level of  $10^{-6}$  can drastically affect the computed AUC for the VQC trained using SBS-processed data.

The performance of both optimizers, *Adam* and *TPE*, is usually saturated with only 2 layers. This effect is most noticeable when the number of features is greater or equal to 3. By filtering only the PCA-obtained results, both optimizers are compatible with most of the results. An exception is observed when using a higher number of features ( $\geq 4$ ) and only one layer, with the *TPE*'s performance being better, and in the remaining cases when using a higher number of features ( $\geq 4$ ), where the opposite happens and *Adam* outperforms *TPE*.

For the best set of HP, both VQC trained using *Adam* and *TPE* have a performance compatible with the performance obtained using Shallow ML methods (c.f. with Figure 10 and Figure 12, respectively). It was also observed that there are no cases where QML outperforms both the shallow methods tested. Furthermore, it was seen that the best-performant model originated from the *TPE* optimizer, with an AUC score of 0.92.

The shallow ML methods results, trained on the same data as the VQC, are shown in Figure 4. The AUC scores obtained in this case are more stable for both the PCA and SBS datasets. The performance in both cases is saturated when using 2 features and the models trained with SBS data outperform the PCA-trained models, contrary to what was observed for the QML case. It should also be noted that the SVM outperforms LR in all cases except when only one feature is used, which is not surprising since SVMs are more sophisticated classifiers.

### 8.2 Dataset Reduction

In order to provide a benchmark point for comparison with the performance of the reduced datasets, a LR model was trained with the full dataset. Subsequently, a different number of  $k$  features ( $k \in [1, 2, 3, 4, 5]$ ) were selected with the SBS algorithm. The corresponding AUC scores are shown in Table 6.

The performance of the *KMeans* algorithm was tested by training a LR model with 10 datasets obtained from the reduction of the original one using random undersampling<sup>5</sup>. The mean AUC score and respective standard deviation found using this method are summarised in Figure 5. The framework presented in subsection 6.1 was applied to the training dataset and several test datasets were obtained through random

<sup>5</sup>Throughout this article random undersampling refers to the random selection of data points from the original dataset.

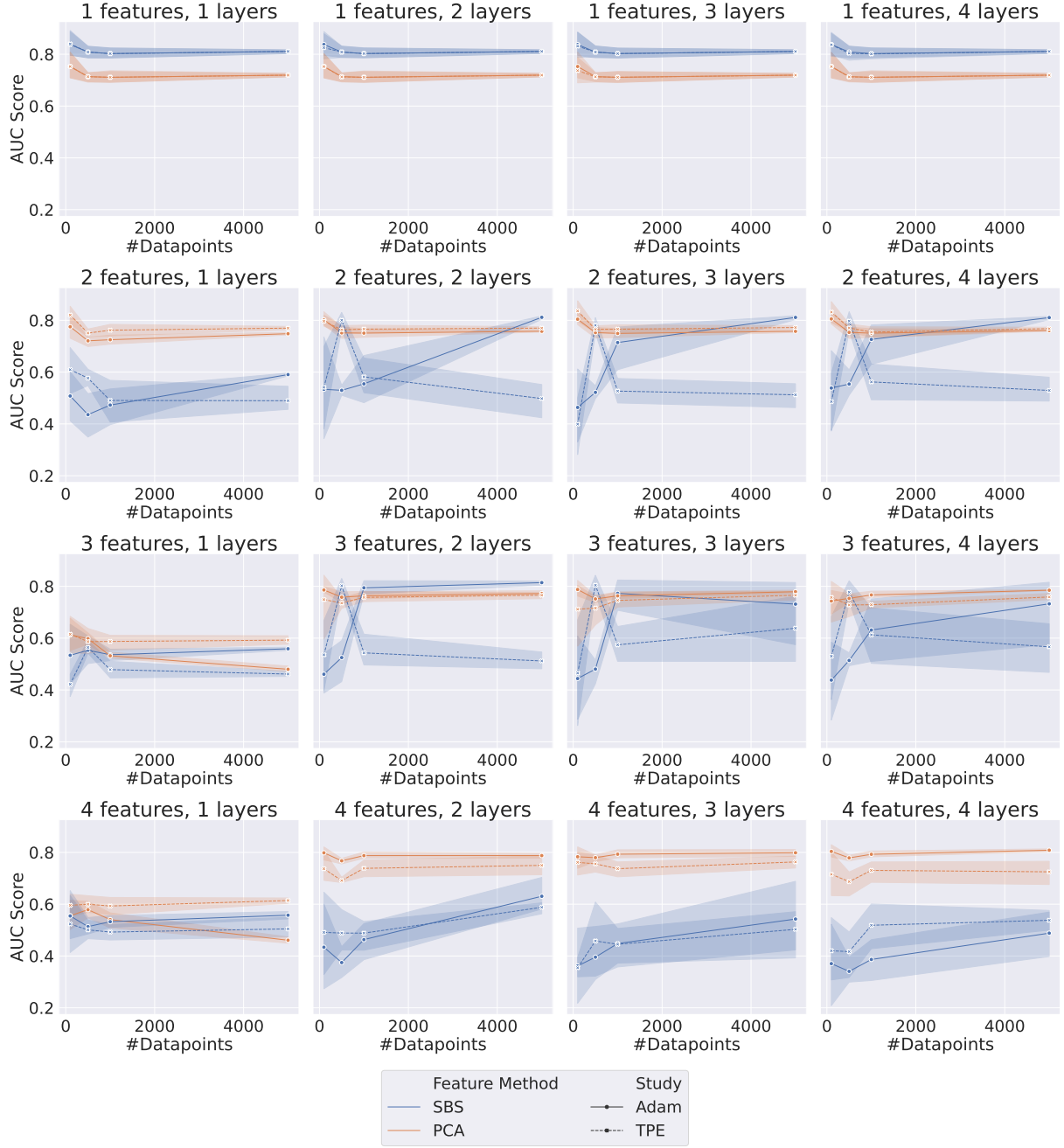


Figure 3: Plot grid representing the results for both *Adam* and *TPE*-Trained VQCs. Each data point represents the AUC score on the test dataset of a different set of HPs as listed in Table 5. The error bar represents the standard deviation associated with each data point since each point is the average of 5 different random samplings from the data.

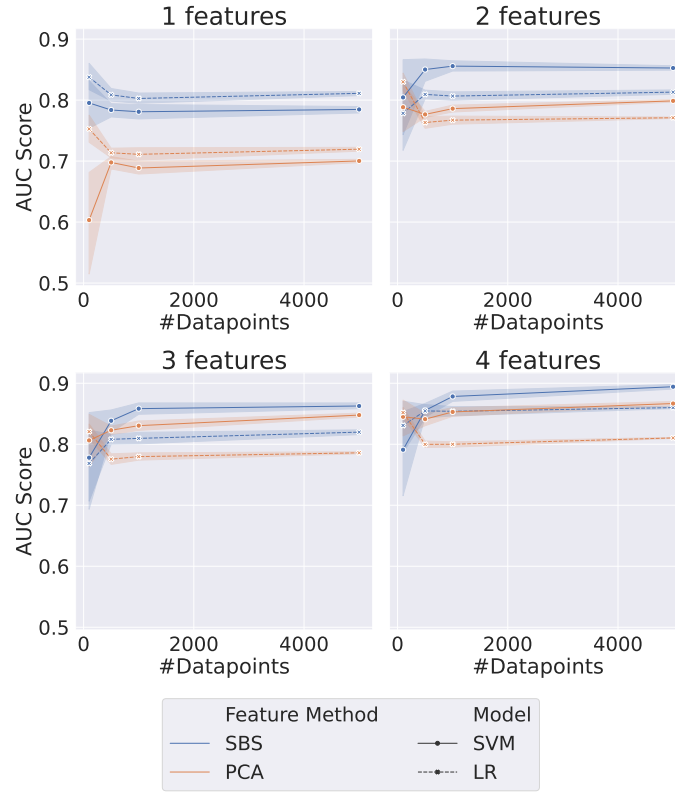


Figure 4: Plot grid representing the results for the considered shallow methods. Each data point represents the AUC score on the test dataset of a different set of HPs as listed in Table 5. The error bar represents the standard deviation associated with each data point since each point is the average of 5 different random samplings from the data.

Number of features	AUC Score
1	0.818
2	0.818
3	0.824
4	0.845
5	0.865

Table 6: Ideal scenario AUC scores. AUC scores were obtained by training a logistic regression with the full dataset, for the different number of features.

undersampling. The *KMeans* algorithm considered the samples' weight and, in order to have an equal number of signal and background centroids, was separately applied to the signal and background data. Since state-of-the-art quantum computing requires small datasets, the data reduction studies were done for datasets with 100, 500, 1000, and 5000 data points and the number of features previously mentioned.

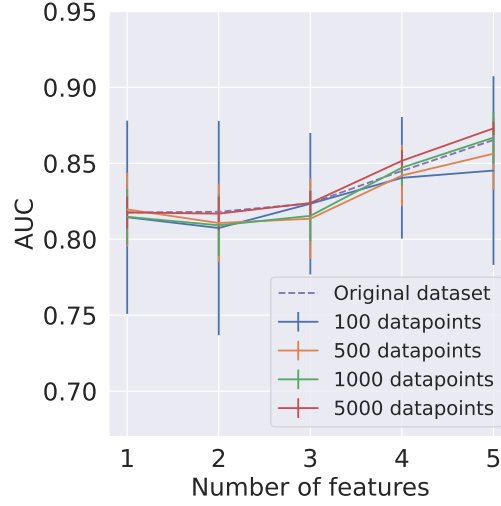


Figure 5: Average AUC score and corresponding standard deviation, represented as uncertainty bands, for different numbers of clusters as a function of the number of features. Train and test datasets were reduced with random undersampling. For each case were used 10 different reduced datasets.

The results obtained using the *KMeans* algorithm in the training dataset and random undersampling in the test signal and background samples are presented in [Figure 6](#).

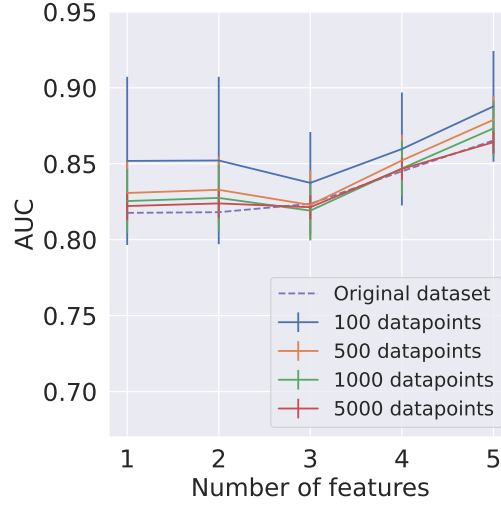


Figure 6: Average AUC score and corresponding standard deviation, represented as uncertainty bands, for different numbers of clusters as a function of the number of features. The training dataset was reduced using the *KMeans* algorithm. For each case were used 10 different randomly undersampled test datasets.

It can be seen in [Figure 5](#) and [Figure 6](#) that when using the *KMeans* algorithm to reduce the training dataset the AUC scores slightly improve in general, although both results are compatible. This study shows that even if the *KMeans* algorithm is a more sophisticated algorithm for data reduction, for the HEP case being considered no significant deterioration of the performance is observed, suggesting that the dataset composed of prototypes is a good representative of the whole dataset in this study.

### 8.3 Performance Studies

The QML, SVM, and LR models were trained with *TPE* for both the random undersampling and the *KMeans* reduced datasets for different dataset sizes. In this comparison, the other tested HP are SBS for the feature method, 1 feature, and 5 VQC layers, corresponding to the best set of HP previously found. The metric used to compare is the AUC score average of 5 different runs. Since only the train dataset was reduced using this method, the test set was reduced using random undersampling, hence for each dataset size, there is 1 train, 5 validation, and 5 test datasets. The choice to keep random sampling for the validation and test sets is to ensure that our methodology represents the test as close to approximation as possible, ensuring that sophisticated resampling techniques are not affecting this.

The obtained results are shown in [Figure 7](#). It can be seen that, as expected from the results discussed in [subsection 8.2](#), the performance for *KMeans* reduced dataset is compatible to the obtained with the dataset reduced through random undersampling.

Nonetheless, it should be emphasized that the model trained with random undersampling needs to be trained several times for achieving these average scores, as many times as the number of reduced datasets used. On the other hand, the models using the *KMeans* reduced dataset need to be trained only once. This can be relevant in the context of quantum computers, where access is often subject to long queues and thus the number of accesses can be a limiting factor.

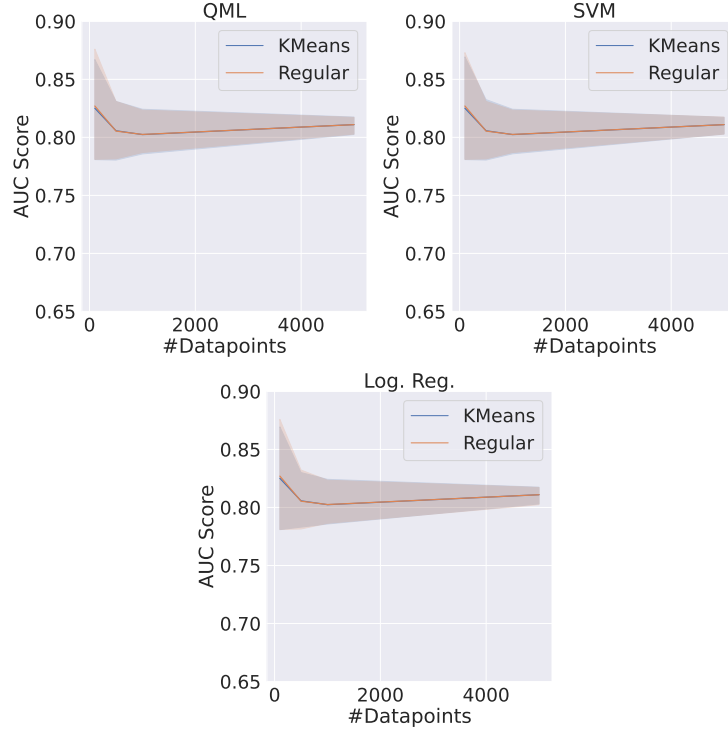


Figure 7: Comparison between the QML, SVM, and logistic regression models when trained with the *TPE* and the best set of HP for different dataset sizes for both random undersampling (regular) and *KMeans* reduced datasets.

## 9 Real Quantum Computers Results

Until this point, only simulated quantum environments were used. In order to test the performance in real quantum computers, and thus validate the simulation results, the *PennyLane* framework was used as the integration layer with *Qiskit*, which works effectively as a direct API to the quantum computers provided by IBM.

In this study only the best performant model HP-set was used, *i.e.* the *TPE*-Trained VQC. This VQC was implemented and its test set was inferred on 6 different quantum systems, all of them freely available. IBM's transpiler optimization level was set to 3 [47] and, for each event, the final expectation value was computed by averaging 20k shots on the quantum computer. The obtained results, shown in [Figure 8](#), are compatible with the simulated ones.

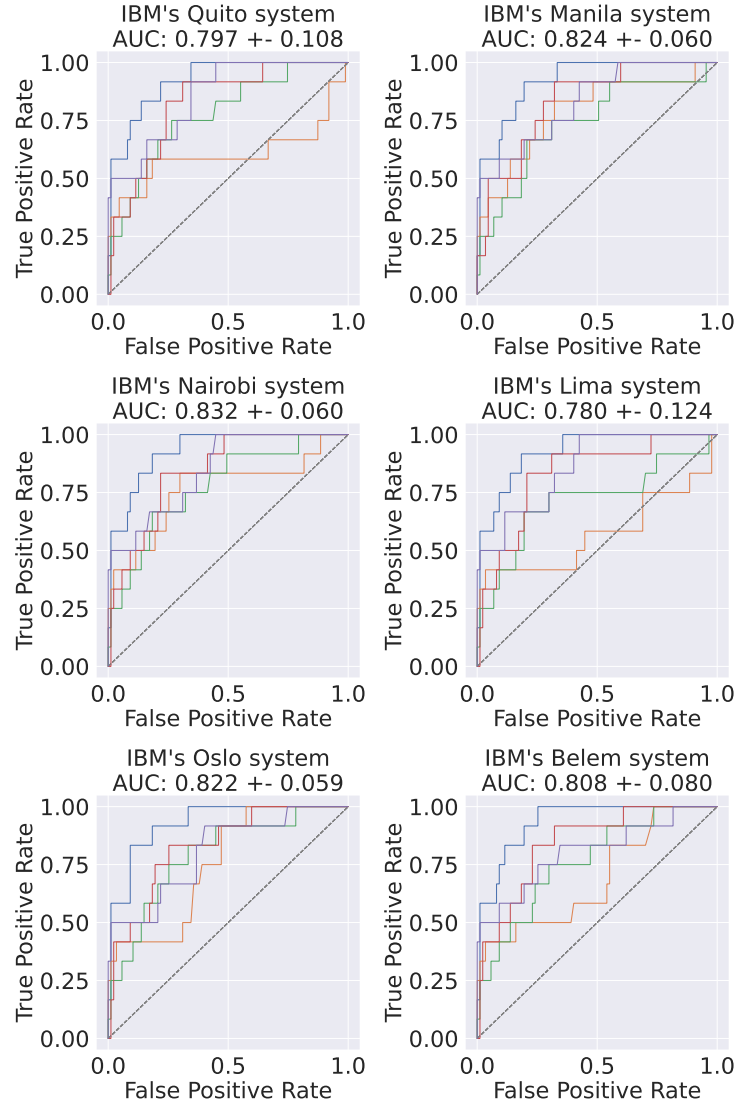


Figure 8: Final ROC curve of the best-performing model when inferred on the test dataset in 6 different IBM systems. The average AUC scores and the corresponding standard deviations are also shown.

## 10 Conclusion

In the current article, the feasibility of QML techniques applied to HEP data was assessed in a consistent way. Shallow classical methods were used for the performance comparison with QML since deep methods are known to require large datasets, which are not viable given the limitations of the current quantum computers.

Feature selection techniques were addressed and it was shown that even if SBS is a commonly used technique, in the HEP case under study, this method yielded overall worst and more unstable results when compared to PCA. This might point out that PCA-transformed data suits QML applications better in the HEP context.

More sophisticated data reduction techniques, such as the KMeans algorithm, produced results compatible with the ones found when using random undersampling. This can be relevant in the context of QML since it means that it is possible to achieve the same results by training the model just one time, thus reducing the number of accesses to the quantum computer.

The performed grid search performance provided no evidence of quantum advantage for the HEP case under study. The best performant configuration was also run on several real-world quantum systems and provided compatible results with simulated circuits, validating the obtained results.

It was also shown that a black-box optimizer such as *TPE* can achieve competitive results compared to a well-established optimizer such as *Adam* in QML. This advantage is twofold since *TPE* does not compute gradients (and thus there is no need for backpropagation), providing a significant speedup in the training time and used memory.

## Acknowledgments

We acknowledge the use of IBM Quantum services for this work. The views expressed are those of the authors, and do not reflect the official policy or position of IBM or the IBM Quantum team.

This work was supported by Fundação para a Ciência e a Tecnologia, Portugal, through project CERN/FIS-COM/0004/2021 (“Exploring quantum machine learning as a tool for present and future high energy physics colliders”).

We thank Declan Millar, Nuno Peres and Tiago Antão for the very useful discussions and Ricardo Ribeiro for kindly providing access to some of the computing systems used in this work. We also thank Henrique Carvalho for the help in producing [Figure 1](#).

## Appendix

The code used in this work is publicly available in <https://github.com/mcpeixoto/QML-HEP>.

The results of the *Adam*-Trained VQCs are shown in [Figure 9](#), while [Figure 10](#) shows the ROC curves for the the best HP set. The corresponding results for *TPE* are shown in [Figure 11](#) and [Figure 12](#).

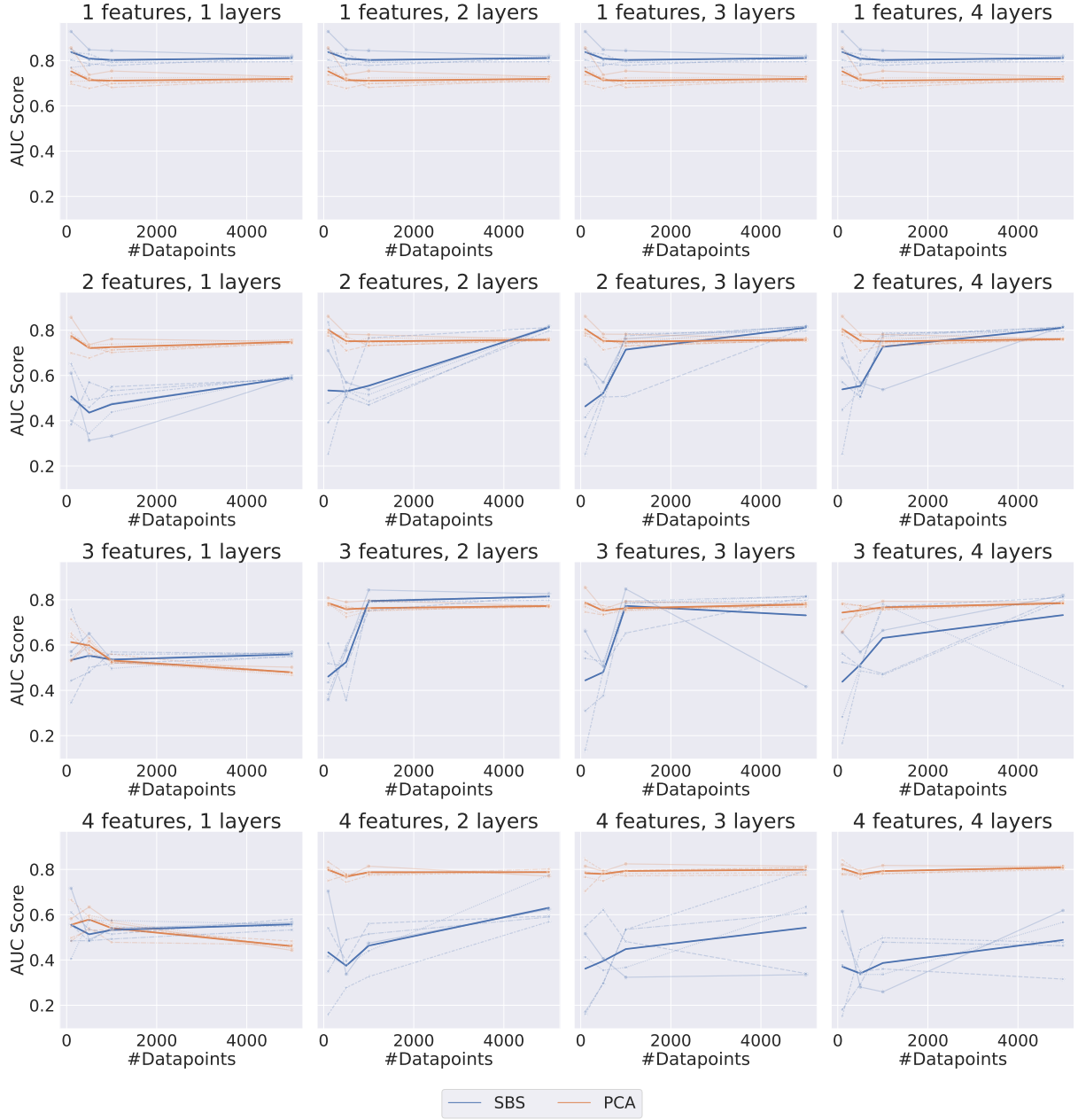


Figure 9: Plot grid containing the results of *Adam*-Trained VQCs. There are 5 semi-transparent data points for each value of the x-axis, representing the 5 different random samplings from the data. Each value of the x-axis also represents a different set of HP deduced from the Table 5. The full-colored lines are the average values of these runs. On the grid system on the x-axis, the number of layers is varied and on the y-axis, the number of features.

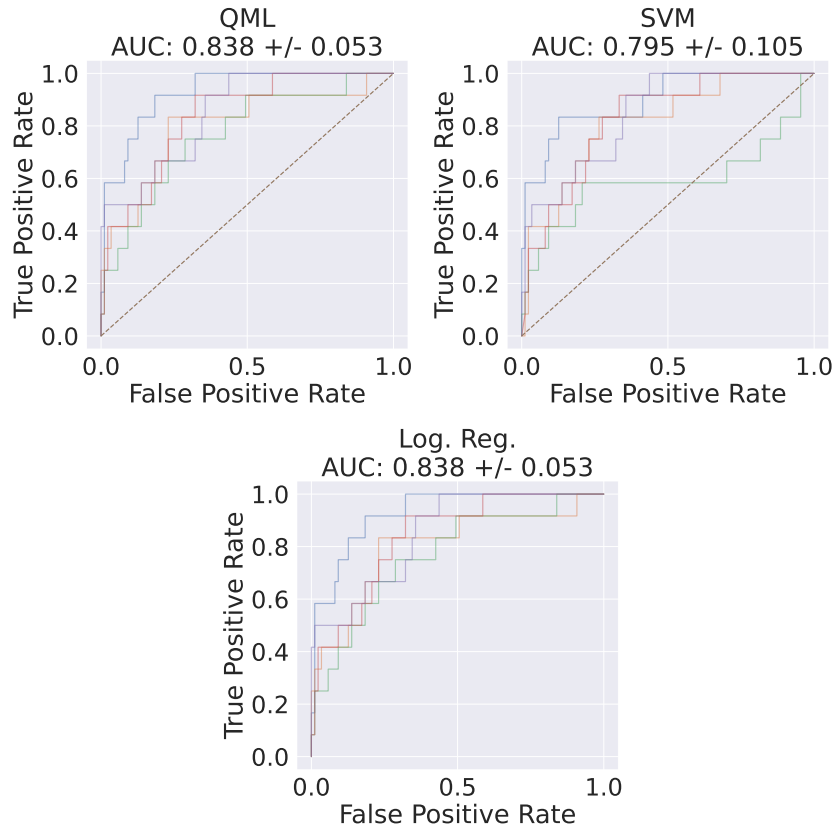


Figure 10: ROC of the best HP set, using *Adam*'s QML model average AUC score as a metric, and the corresponding shallow methods ROCs for the same data. The HP for this run are SBS for feature method, 100 data points, 1 feature, and 1 VQC layer.

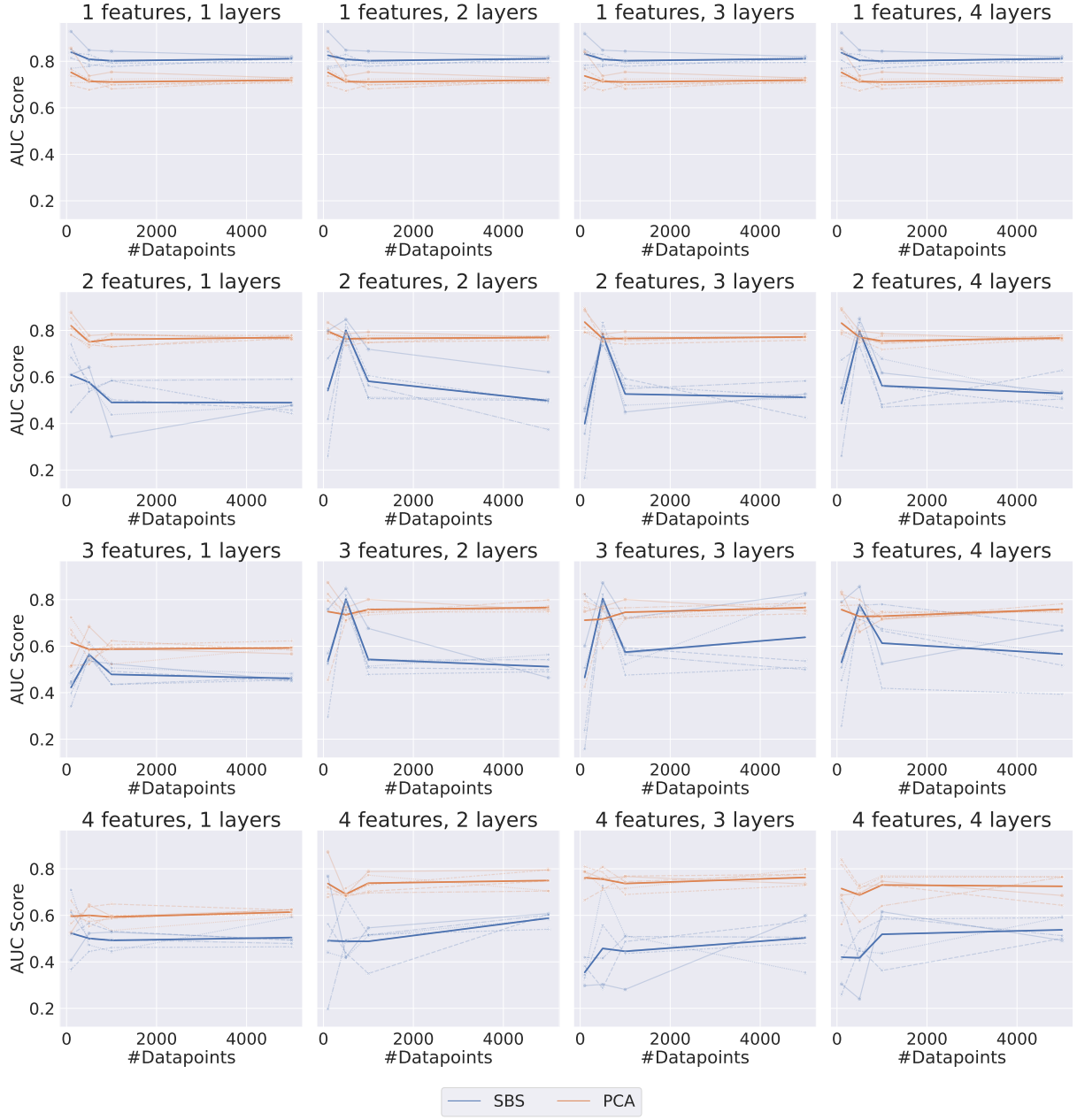


Figure 11: Plot grid containing the results of *TPE*-Trained VQCs. There are 5 semi-transparent data points for each value of the x-axis, representing the 5 different random samplings from the data. Each value of the x-axis also represents a different set of HP, deducted from the [Table 5](#). The full-colored lines are the average values of these runs. On the grid system on the x-axis, the number of layers is varied and on the y-axis, the number of features.

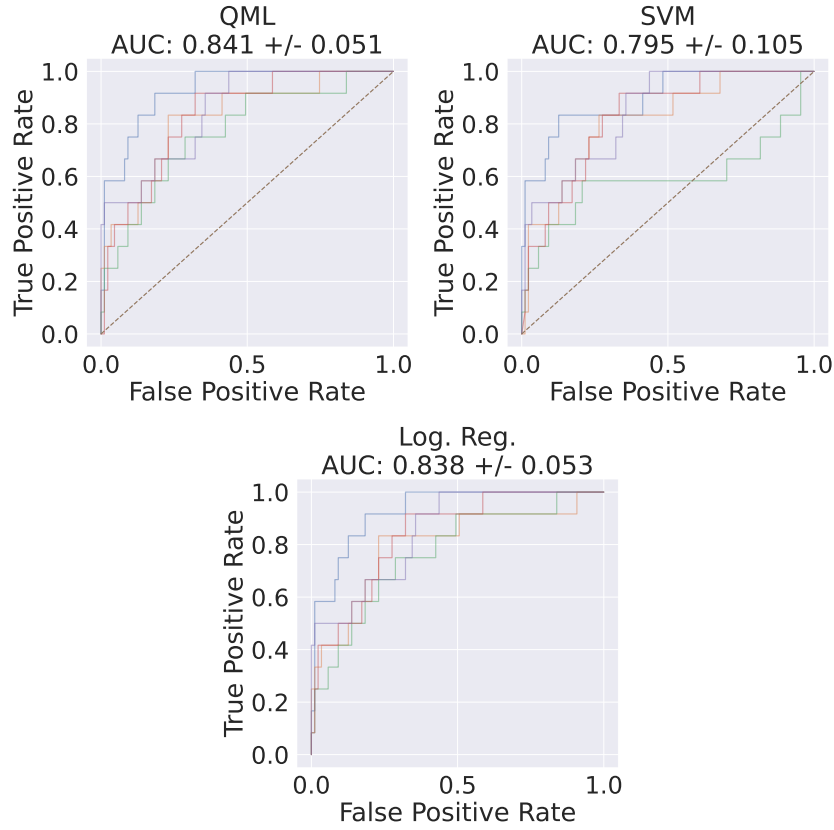


Figure 12: ROC of the best HP set, using *TPE*'s QML model average AUC score as a metric, and the corresponding shallow methods ROCs for the same data. The HP for this run are SBS for feature method, 100 data points, 1 feature and 5 VQC layers.

## References

- [1] J. Ellis, *Outstanding questions: Physics beyond the Standard Model*, Phil. Trans. Roy. Soc. Lond. A **370**, 818 (2012).
- [2] D. Guest, K. Cranmer and D. Whiteson, *Deep learning and its application to LHC physics*, Ann. Rev. Nucl. Part. Sci. **68**, 161 (2018).
- [3] M. Feickert and B. Nachman, *A Living Review of Machine Learning for Particle Physics* (2021), [2102.02770](#).
- [4] I. Shapoval and P. Calafiura, *Quantum associative memory in hep track pattern recognition*, In *EPJ Web of Conferences*, vol. 214, p. 01012. EDP Sciences (2019).
- [5] C. Tüysüz, F. Carminati, B. Demirköz, D. Dobos, F. Fracas, K. Novotny, K. Potamianos, S. Vallecorsa and J.-R. Vlimant, *Particle track reconstruction with quantum algorithms*, In *EPJ Web of Conferences*, vol. 245, p. 09013. EDP Sciences (2020).

- [6] F. Bapst, W. Bhimji, P. Calafiura, H. Gray, W. Lavrijsen, L. Linder and A. Smith, *A pattern recognition algorithm for quantum annealers*, Computing and Software for Big Science **4**(1), 1 (2020).
- [7] L. Funcke et al., *Studying quantum algorithms for particle track reconstruction in the LUXE experiment* (2022), [2202.06874](#).
- [8] A. Zlokapa, A. Anand, J.-R. Vlimant, J. M. Duarte, J. Job, D. Lidar and M. Spiropulu, *Charged particle tracking with quantum annealing optimization*, Quantum Machine Intelligence **3**(2), 1 (2021).
- [9] S. Das, A. J. Wildridge, S. B. Vaidya and A. Jung, *Track clustering with a quantum annealer for primary vertex reconstruction at hadron colliders* (2019), [1903.08879](#).
- [10] A. Y. Wei, P. Naik, A. W. Harrow and J. Thaler, *Quantum algorithms for jet clustering*, Physical Review D **101**(9), 094015 (2020).
- [11] A. Mott, J. Job, J.-R. Vlimant, D. Lidar and M. Spiropulu, *Solving a higgs optimization problem with quantum annealing for machine learning*, Nature **550**(7676), 375 (2017).
- [12] A. Zlokapa, A. Mott, J. Job, J.-R. Vlimant, D. Lidar and M. Spiropulu, *Quantum adiabatic machine learning with zooming*, Bulletin of the American Physical Society **66** (2021).
- [13] K. Terashi, M. Kaneda, T. Kishimoto, M. Saito, R. Sawada and J. Tanaka, *Event classification with quantum machine learning in high-energy physics*, Computing and Software for Big Science **5**(1), 1 (2021).
- [14] S. L. Wu, S. Sun, W. Guan, C. Zhou, J. Chan, C. L. Cheng, T. Pham, Y. Qian, A. Z. Wang, R. Zhang et al., *Application of quantum machine learning using the quantum kernel algorithm on high energy physics analysis at the LHC*, Physical Review Research **3**(3), 033221 (2021).
- [15] A. Blance and M. Spannowsky, *Quantum machine learning for particle physics using a variational quantum classifier*, Journal of High Energy Physics **2021**(2), 1 (2021).
- [16] V. S. Ngairangbam, M. Spannowsky and M. Takeuchi, *Anomaly detection in high-energy physics using a quantum autoencoder*, Physical Review D **105**(9), 095004 (2022).
- [17] A. Gianelle, P. Koppenburg, D. Lucchesi, D. Nicotra, E. Rodrigues, L. Sestini, J. de Vries and D. Zuliani, *Quantum Machine Learning for b-jet charge identification*, JHEP **08**, 014 (2022), doi: 10.1007/JHEP08(2022)014, [2202.13943](#).
- [18] S. Y.-C. Chen, T.-C. Wei, C. Zhang, H. Yu and S. Yoo, *Quantum convolutional neural networks for high energy physics data analysis*, Physical Review Research **4**(1), 013231 (2022).
- [19] V. Belis, S. González-Castillo, C. Reissel, S. Vallecorsa, E. F. Combarro, G. Dissertori and F. Reiter, *Higgs analysis with quantum classifiers*, In EPJ Web of Conferences, vol. 251, p. 03070. EDP Sciences (2021).
- [20] J. Preskill, *Quantum computing in the NISQ era and beyond*, Quantum **2**, 79 (2018), doi:10.22331/q-2018-08-06-79.
- [21] G. Li, Y. Ding and Y. Xie, *Tackling the qubit mapping problem for nisq-era quantum devices*, doi: 10.48550/ARXIV.1809.02573 (2018).
- [22] S. Gupta and R. Zia, *Quantum neural networks*, Journal of Computer and System Sciences **63**(3), 355 (2001).

- [23] M. Schuld, I. Sinayskiy and F. Petruccione, *Simulating a perceptron on a quantum computer*, Physics Letters A **379**(7), 660 (2015).
- [24] E. Farhi and H. Neven, *Classification with quantum neural networks on near term processors* (2018), [1802.06002](#).
- [25] M. Schuld, A. Bocharov, K. M. Svore and N. Wiebe, *Circuit-centric quantum classifiers*, Physical Review A **101**(3) (2020), doi:10.1103/physreva.101.032308.
- [26] R. LaRose and B. Coyle, *Robust data encodings for quantum classifiers*, Physical Review A **102**(3), 032420 (2020).
- [27] F. Pedregosa, G. Varoquaux, A. Gramfort, V. Michel, B. Thirion, O. Grisel, M. Blondel, P. Prettenhofer, R. Weiss, V. Dubourg, J. Vanderplas, A. Passos *et al.*, *Scikit-learn: Machine learning in Python*, Journal of Machine Learning Research **12**, 2825 (2011).
- [28] M. Crispim Romao, N. F. Castro and R. Pedro, *Simulated pp collisions at 13 TeV with 2 leptons + 1 b jet final state and selected benchmark Beyond the Standard Model signals*, Dataset on Zenodo, doi:10.5281/zenodo.5126747 (2021).
- [29] M. Crispim Romão, N. F. Castro and R. Pedro, *Finding New Physics without learning about it: Anomaly Detection as a tool for Searches at Colliders*, Eur. Phys. J. C **81**(1), 27 (2021), doi:10.1140/epjc/s10052-021-09813-2, [Erratum: Eur.Phys.J.C 81, 1020 (2021)], [2006.05432](#).
- [30] G. Durieux, F. Maltoni and C. Zhang, *Global approach to top-quark flavor-changing interactions*, Phys. Rev. D **91**(7), 074017 (2015), doi:10.1103/PhysRevD.91.074017, [1412.7166](#).
- [31] J. Alwall, R. Frederix, S. Frixione, V. Hirschi, F. Maltoni, O. Mattelaer, H. S. Shao, T. Stelzer, P. Torrielli and M. Zaro, *The automated computation of tree-level and next-to-leading order differential cross sections, and their matching to parton shower simulations*, JHEP **07**, 079 (2014), doi:10.1007/JHEP07(2014)079, [1405.0301](#).
- [32] T. Sjöstrand, S. Ask, J. R. Christiansen, R. Corke, N. Desai, P. Ilten, S. Mrenna, S. Prestel, C. O. Rasmussen and P. Z. Skands, *An introduction to PYTHIA 8.2*, Comput. Phys. Commun. **191**, 159 (2015), doi:10.1016/j.cpc.2015.01.024, [1410.3012](#).
- [33] M. Selvaggi, *DELPHES 3: A modular framework for fast-simulation of generic collider experiments*, J. Phys. Conf. Ser. **523**, 012033 (2014), doi:10.1088/1742-6596/523/1/012033.
- [34] M. Cacciari, G. P. Salam and G. Soyez, *The anti- $k_t$  jet clustering algorithm*, JHEP **04**, 063 (2008), doi:10.1088/1126-6708/2008/04/063, [0802.1189](#).
- [35] J. Thaler and K. Van Tilburg, *Identifying boosted objects with n-subjettiness*, Journal of High Energy Physics **2011**(3), 1 (2011).
- [36] T. Chen and C. Guestrin, *XGBoost: A scalable tree boosting system*, In *Proceedings of the 22nd ACM SIGKDD International Conference on Knowledge Discovery and Data Mining*, KDD '16, pp. 785–794. ACM, New York, NY, USA, ISBN 978-1-4503-4232-2, doi:10.1145/2939672.2939785 (2016).
- [37] S. Raschka, *Mlxtend: Providing machine learning and data science utilities and extensions to python's scientific computing stack*, The Journal of Open Source Software **3**(24) (2018), doi:10.21105/joss.00638.

- [38] D. MacKay, *Information Theory, Inference and Learning Algorithms*, Cambridge University Press (2003).
- [39] G. A. Wilkin and H. Xiuzhen, *A practical comparison of two k-means clustering algorithms*, BMC bioinformatics **9** (2008), doi:10.1186/1471-2105-9-S6-S19.
- [40] A. Vouros, S. Langdell, M. Croucher and E. Vasilaki, *An empirical comparison between stochastic and deterministic centroid initialisation for k-means variations*, Machine Learning **110**, 1975 (2021), doi:10.1007/s10994-021-06021-7.
- [41] D. P. Kingma and J. Ba, *Adam: A Method for Stochastic Optimization* (2014), [1412.6980](#).
- [42] J. Bergstra, R. Bardenet, Y. Bengio and B. Kégl, *Algorithms for hyper-parameter optimization*, Advances in neural information processing systems **24** (2011).
- [43] J. Bergstra, D. Yamins and D. Cox, *Making a science of model search: Hyperparameter optimization in hundreds of dimensions for vision architectures*, In *International conference on machine learning*, pp. 115–123. PMLR (2013).
- [44] T. Akiba, S. Sano, T. Yanase, T. Ohta and M. Koyama, *Optuna: A next-generation hyperparameter optimization framework*, In *Proceedings of the 25rd ACM SIGKDD International Conference on Knowledge Discovery and Data Mining* (2019).
- [45] F. A. de Souza, M. Crispim Romão, N. F. Castro, M. Nikjoo and W. Porod, *Exploring Parameter Spaces with Artificial Intelligence and Machine Learning Black-Box Optimisation Algorithms* (2022), [2206.09223](#).
- [46] V. Bergholm et al., *PennyLane: Automatic differentiation of hybrid quantum-classical computations* (2018), [1811.04968](#).
- [47] M. S. ANIS, Abby-Mitchell, H. Abraham, AduOffei, R. Agarwal, G. Agliardi, M. Aharoni, I. Y. Akhalwaya, G. Aleksandrowicz, T. Alexander, M. Amy, S. Anagolum et al., *Qiskit: An open-source framework for quantum computing*, doi:10.5281/zenodo.2573505 (2021).